

# MAKING, BREAKING AND SLIDING OF NANOMETER-SCALE CONTACTS

*References have been updated from the original publication in this document.*

R.W. CARPICK\*, M. ENACHESCU, D.F. OGLETREE, M. SALMERON

Materials Sciences Division, Lawrence Berkeley National Laboratory, Berkeley, CA 94720.

\* present address: Sandia National Laboratories, MS1413, Albuquerque, NM 87185-1413, rwcarki@sandia.gov

## ABSTRACT

The contact between an atomic force microscope tip and a sample surface can form an ideal single asperity of nanometer dimensions, where the interaction forces can be measured with sub-nanoNewton force resolution. Studies of contact, adhesion and friction for these nano-asperities have been carried out for a variety of tips and single crystal sample surfaces. The major result is the observation of proportionality between friction and true contact area for a variety of systems, and an impressive agreement with continuum mechanics models for contact area even at the nanometer scale. The relevant continuum models can in fact be understood in the framework of fracture mechanics.

## INTRODUCTION

As devices shrink in size, the increased surface-to-volume ratio of the component materials ensures that interfacial forces such as friction and adhesion can play dominant roles. This fact is painfully appreciated by the designers of microelectromechanical systems (MEMS) who often observe catastrophic failure of MEMS devices due to adhesion, friction and resultant wear. Understanding these interfacial forces should allow such problems to be remedied, and furthermore, the relative strength of these forces could potentially be exploited for specific micro- and nano-scale device applications.

There is currently no fundamental theory that explains or predicts friction in general. At the macroscopic level, it is almost universally observed that the friction force ( $F_f$ ) is linearly proportional to the normal force or load ( $L$ ):

$$F_f = \mu \cdot L \quad (1)$$

which defines the friction coefficient  $\mu$ . Eq. (1) is often referred to as Amonton's Law. Macroscopic studies are generally hindered by the inevitable roughness of typical surfaces (fig. 1). A complex multitude of contact points at the interface ensures that the true contact area is much smaller than the apparent contact area, and is nearly impossible to determine. Other factors, such as wear, third-bodies and tribochemistry further complicate the matter.

The atomic force microscope (AFM) is an ideal tool with which to study contact and friction in a fundamental way[1]. A tip, with typically 10-100 nm radius of curvature, is attached to a compliant cantilever spring. At low applied loads, the tip can form a nanometer-scale single contact point (an "asperity") with a variety of sample surfaces, thus providing a well-defined interface (fig. 1). The cantilever deflections are recorded using, most commonly, a reflected optical beam. These deflections are converted to forces by using Hooke's Law. In principle, the normal and lateral forces can be measured with sub-nanoNewton precision, with sub-Ångstrom displacement precision. This tip is rastered over the surface using piezoelectric scanning tubes. In practice, numerous issues such as cantilever calibration, non-linear piezoelectric scanning components, thermal drift, and coupling of bending modes put limits on the accuracy of these

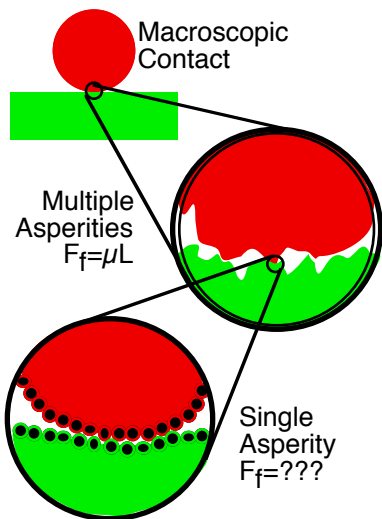


Fig. 1. The typical surface roughness of macroscopic interfaces ensures a complex multitude of contact points (asperities). A scanning probe instrument provides a well-defined single asperity contact (the tip) where interaction forces can be precisely measured with nanometer/atomic resolution. At this scale, macroscopic physical laws no longer apply. For example, the friction force ( $F_f$ ) is no longer linearly proportional to the applied load ( $L$ ).

measurements. These issues have been discussed previously[2] and will only be briefly mentioned in this paper.

## EXPERIMENT

The atomic force microscope used in these experiments is described elsewhere[3]. It operates in ultrahigh vacuum (UHV) to ensure surface cleanliness. Chamber pressures were in the  $10^{-10}$  Torr regime or better. Experiments were performed at room temperature. Microfabricated cantilevers from commercial vendors were used. Scanning electron microscopy measurements of cantilever dimensions were combined with continuum elasticity theory calculations to estimate the normal force spring constants. Lateral forces were calibrated with respect to the normal forces using the “wedge calibration technique”[2]. Briefly, the relative lateral-to-normal force sensitivity ratio is experimentally determined by observing the cantilever’s bending response on a tilted surface, *i.e.* by imposing a

geometrically determined lateral force.

The tip geometry was experimentally determined using “inverse imaging”. By scanning the tip in contact with a much sharper feature on the sample, the tip’s profile can be determined. This is accomplished by scanning the tip over the atomically-sharp facets of a  $\text{SrTiO}_3(305)$  faceted surface[4,5], providing a tip cross-section. Unless otherwise noted, the tip was determined to be paraboloidal. The influence of tip geometry is discussed in the next section.

A variety of interfaces were examined with this apparatus:

(1) A platinum-coated tip and a muscovite mica(0001) sample[4,6]. The 100 nm Pt coating was deposited by sputtering onto a plasma-cleaned silicon nitride cantilever. Continuity of the Pt coating was determined by measuring substantial contact conductance between the tip and a conducting sample. Muscovite mica was cleaved inside the vacuum chamber just prior to the experiment, producing large step-free regions for measurement.

(2) A silicon nitride tip and a muscovite mica(0001) sample. The tip and cantilever are fabricated from low-stress LPCVD silicon nitride which is non-stoichiometric. These  $\text{SiN}_x$  cantilevers were used as-received from the vendor (Park Scientific Instruments, Sunnyvale CA). Scanning Auger electron spectroscopy measurements indicate that the surface terminates in a layer with appreciable oxygen content along with Si and N.

(3) A tungsten-carbide (WC) tip and a hydrogen-terminated diamond(111) single-crystal sample[7]. The cantilever was fabricated from Si and coated with  $\sim 20\text{nm}$  of WC (NT-MDT, Moscow, Russia). Auger depth profiles indicated that the WC coating also contains oxygen. The sample was a type II B diamond(111) single crystal (boron doped), saturated with hydrogen in a plasma. Vacuum annealing was used to clean the sample, as described in detail elsewhere[8]. Topographic AFM imaging revealed that the diamond sample consists of flat islands  $\sim 150\text{-}250 \text{ \AA}$

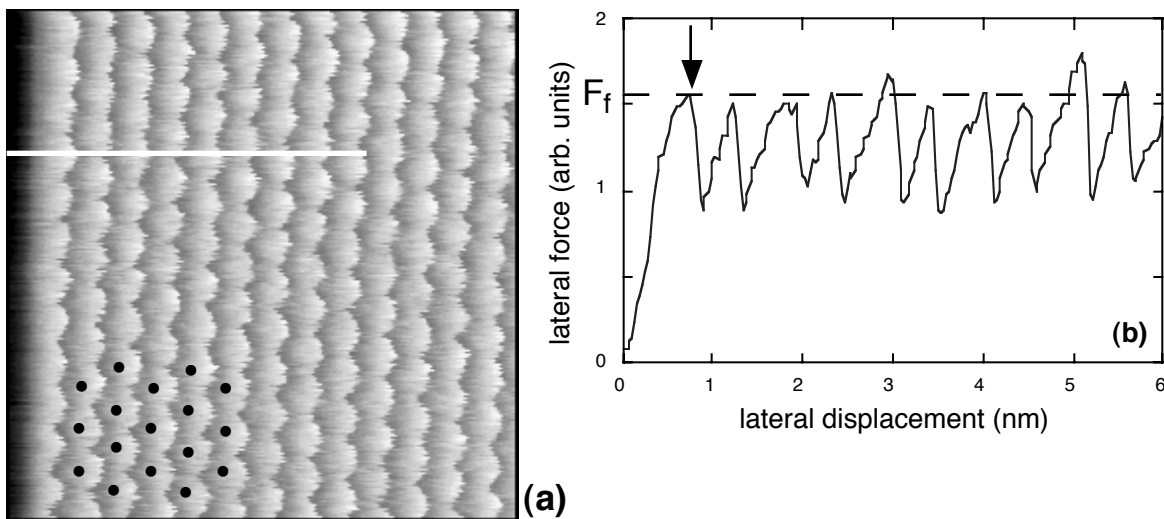


Fig. 2. (a)  $7.5 \times 7.5 \text{ nm}^2$  lateral force image of the mica(0001) surface. The fast scan direction is from left to right. The black dots represent the repeat units of the mica lattice, whose periodicity coincides with the lateral forces. (b) Line trace of the section indicated in (a). The lateral force exhibits “stick-slip” behavior, where the lateral force builds up to some well-defined maximum value, and then quickly relaxes (first arrow). During the relaxation, the tip slips by one unit cell. This behavior repeats itself with the lattice periodicity.

in diameter. A very sharp (1 x 1) LEED pattern was observed, indicating that the islands consist of ordered diamond, which was also verified by previous AFM lattice-resolved imaging[8]. All measurements were performed on these atomically flat islands. The hydrogen termination produces an unreconstructed, passivated (non-reactive) surface.

## RESULTS

### Atomic-Scale Stick-Slip

Frequently, when an AFM tip is placed in contact with a crystalline sample and scanned across it to generate a force map, atomic-scale periodicity is observed (fig. 2a)[9]. Lateral and normal forces are observed to vary with the periodicity of the sample’s lattice. This behavior has been observed for a wide variety of tips and samples, and a wide range of experimental conditions (liquid, ambient, controlled atmosphere, vacuum)[1]. When examined in detail (fig 2b), this behavior is seen to result from discontinuous motion of the tip along the surface. As the lever is continuously rastered across the sample, the tip traces out the sample’s lattice through a regular series of stick-slip events. Theories to explain this phenomena are under development and are not the focus of this paper. We point out that, as seen in fig. 2b, there is a reproducible critical lateral force at which the slip occurs. We are interested in understanding what physical parameters determine this atomic-scale static friction force,  $F_f$ . To do this, we measure the average value of this friction force at a given load, change the load slightly, then measure the friction again, and so on. Typically we measure half of the difference between the average friction force obtained scanning left-to-right and right-to-left, which greatly reduces signal offsets due to coupling of bending modes and optical misalignment. Atomic-scale stick-slip was observed for both the Pt/mica and SiN<sub>x</sub>/mica experiments. It was not observed for the WC/diamond experiment, but this may have been due to the low friction forces for this interface, thus leaving the stick-slip variation within the noise of the measurement.

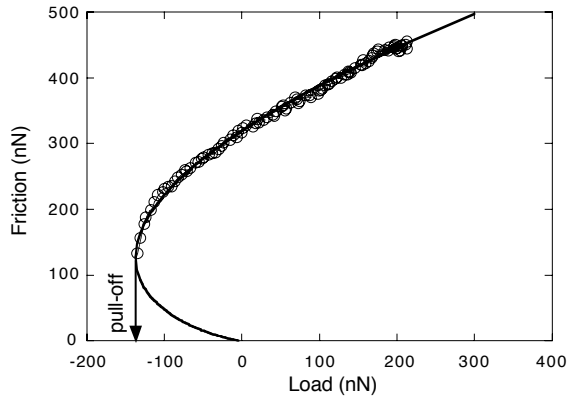


Fig. 3. Friction (circles) vs. externally applied load for a Pt-coated tip in contact with mica in UHV. The tip is initially loaded to  $\sim 210$  nN, then friction is measured as the load is decreased. At  $\sim 140$  nN, the tip pulls out of contact with the sample. The solid line is the JKR prediction for the contact area vs. load, scaled to fit the friction data.

### Pt/Mica Interface: Friction vs. Load

Fig. 3 shows the variation of friction (circles) with load for the Pt/mica interface, measured with decreasing load. Friction is clearly a non-linear function of load, in contradiction with the macroscopic law of Amontons [eq. (1)]. A substantial negative load (called the *pull-off force*) must be applied to separate the tip and sample, at which point finite friction persists. This is an example of the significant role that interfacial forces play in small-scale contacts. In fig. 3, the friction data is well fit by the Johnson-Kendall-Roberts (JKR)[10] model (solid line) for the contact area between adhesive elastic spheres, which is equivalent to the contact geometry between a paraboloidal tip and a flat plane.

The JKR model essentially balances the elastic strain energy with the adhesive interfacial energy to determine the contact area. This model can be derived using fracture mechanics concepts[11,12]. The contact is viewed as an external circular crack in an otherwise infinite medium. The contact edge represents the crack front. Loading and unloading the contact is viewed as propagating this crack (advancing or receding) in mode I (normal separation). Griffith's concept of brittle fracture is used to balance strain energy and interfacial energy to solve for the contact area as a function of load, as summarized elsewhere[11]. The end result is a fairly simple, analytic equation:

$$A = \pi \left( \frac{3R}{4E^*} \right)^{2/3} \left( L + 3\pi\gamma R + \sqrt{6\pi\gamma RL + (3\pi\gamma R)^2} \right)^{2/3} \quad (2)$$

where  $A$  is the contact area,  $R$  is the tip radius,  $\gamma$  is the interfacial energy per unit area (also known as the work of adhesion).  $E^*$  is the reduced Young's modulus of the tip and sample materials, given by

$$E^* = \left( \frac{1-\nu_1^2}{E_1} + \frac{1-\nu_2^2}{E_2} \right)^{-1} \quad (3)$$

where  $E_1, E_2$  are the Young's moduli of the tip and sample respectively, and  $\nu_1, \nu_2$  the respective Poisson's ratios. The JKR relation requires that the tip is paraboloidal. Inverse imaging, described above, verifies that the tip is paraboloidal with a curvature radius of  $\sim 140$  nm.

Since the JKR contact area varies with load in almost exact proportion to the measured friction, we postulate that

$$F_f = \tau \cdot A \quad (4)$$

where  $\tau$  is the interfacial shear strength. Eq. (4) thus represents the essential relation governing friction for an elastic single asperity.

We further tested the validity of the JKR approach by deliberately altering the tip shape through application of an extremely high load while sliding. A blunt, flat tip was produced in this fashion, as verified by inverse imaging. The JKR prediction for contact area will obviously

Table 1

interface	$\gamma$ (mJ/m <sup>2</sup> )	$\tau$ (MPa)	contact radius @ $L=0$ (nm)
Pt/mica	404	910	13.7
SiN <sub>x</sub> /mica	24	52	8.4
WC/Diamond	10	238	1.1

depend upon the tip geometry. We confirmed that the observed friction-load data was well fit by a modified JKR model derived using an appropriately flat tip profile[4].

By using bulk values for the elastic constants ( $E_{mica} = 56.5$  GPa,  $\nu_{mica} = 0.098$ [13],  $E_{Pt} = 177$  GPa,  $\nu_{Pt} = 0.39$ [14]), we can solve for the contact radius at zero load, listed in Table 1. We see that indeed the contact is of nanometer dimensions. Smaller contacts can be formed with smaller tips and less strongly adhering materials. The JKR analysis also allows us to determine both the interfacial energy ( $\gamma$ ) and the shear strength ( $\tau$ ) for this interface (Table 1). The values quoted are for the maximum shear strength and adhesion energy observed for this system; a gradual decrease of both of these ensued due to contact-induced changes in the tip chemistry, as described elsewhere[6]. The adhesion energy (derived from the pull-off force) is relatively strong, surpassing the van der Waals' energy by an order of magnitude. Likewise, the shear strength is extremely large. The theoretical prediction for the shear strength of a crystalline material in the absence of dislocations is given by  $\sim G/30$ [15] where  $G$  is the shear modulus. We can define an "effective" interfacial shear modulus  $G_{eff} = 2G_{mica}G_{Pt}/(G_{mica} + G_{Pt}) \approx 22.3$  GPa. This gives, for Pt/mica,  $\tau \approx G_{eff}/25$ . The shear strength of this system is thus comparable to the ideal material shear strength[16,17].

This surprising result remains to be fully explained. Recent theoretical modeling by Hurtado and Kim[16,17] using dislocation mechanics suggests that below a critical contact size (in the nm range), strongly adhered contacts should exhibit such ideal shear strengths. The strong attractive forces may create a substantial degree of commensurability of the interfacial atoms, thus producing an interface that is resistant to shear, as in a crystalline material. At this scale, according to the theory, the contact is too small to allow the nucleation of even a single dislocation at the contact edge. Dislocation nucleation is predicted to reduce the shear strength substantially at larger scales. Experiments that test this model more thoroughly are desirable.

### **Limitations in Applying the JKR Theory**

Although the JKR fits to the friction data presented above are convincing, our approach contained the implicit assumption that the shear strength  $\tau$  was not dependent upon load. In fact, load-dependent shear strengths have been observed, although only at larger scales and for different materials[18,19]. It would therefore be desirable to determine whether or not the shear strength varies with load.

Furthermore, the JKR model is not a unique prediction for the behavior of a single asperity[20]. The JKR model assumes that the interfacial attraction has zero spatial range; *i.e.* the system gains energy only when the materials are in direct contact. This approach is reasonable only for relatively compliant, strongly adhering materials exhibiting short-range attraction. Finite

range forces have been modeled by others[21,22], with the extreme opposite limit for stiff, weakly adhering materials with long-range forces described by the Derjaguin-Müller-Toporov (DMT) theory[23]. Intermediate cases are treated by Maugis[22] using a Dugdale crack model. Again, using a mode I fracture mechanics approach, this time with a constant adhesive stress acting over a *finite* distance, Maugis provides an analytic solution that predicts the contact area for the JKR and DMT limits, and for cases in between. Maugis' equations are relatively complicated; a simplified form of the solution has been derived which facilitates fitting this model to experimental data[24]. In any event, for these cases, the contact area varies with load in a significantly different fashion compared with the JKR solution.

Finally, the JKR model assumes only normal loading, thus neglecting any possible effect that the substantial applied lateral force has upon the contact area. Johnson[11] has combined the Dugdale model of Maugis with interacting mode I, II and III fracture mechanics. This theory thus includes the influence of the lateral force upon the contact area, and allows the interaction forces to have a finite range. Using this finite range mixed-mode fracture approach, Johnson predicts that the contact area can be reduced appreciably by partial slip at the contact edge which is induced by the applied lateral force. According to this model, the shape of the area-load relation still resembles the JKR curve, but with different (smaller) absolute values. The model also predicts that the lateral force causes pull-off to occur at a smaller load compared to the direct pull-off force (measured without sliding). This model can be tested with AFM by comparing the direct and sliding pull-off forces. A statistical analysis was conducted for the Pt/mica system, revealing an average reduction of the pull-off force by a factor of 0.89 due to sliding. Using this result, the data presented in fig. 3 can be fit by this modified theory, resulting in an increase of the shear strength by about 20% compared with the JKR fit. While the observed pull-off reduction supports Johnson's model, it is not a direct verification that the contact area itself changes due to sliding.

The above considerations make it clearly desirable to measure the contact area directly. Two different methods to accomplish this are described in the following two sections.

### **SiN<sub>x</sub>/Mica Interface: Lateral Stiffness Measurements**

Contact stiffness is defined as the amount of force per unit displacement required to compress an elastic contact in a particular direction, has the units of N/m, and is essentially the "spring constant" of the contact. Contact stiffness applies both for normal and lateral displacements. The lateral contact stiffness of an axi-symmetric contact,  $k_{contact}$ , is in fact directly proportional to the contact radius  $a$ , given by[25]:

$$k_{contact} = 8 \cdot G^* \cdot a \quad (5)$$

where  $G^* = [(2-\nu_1)/G_1 + (2-\nu_2)/G_2]^{-1}$ . Here  $G_1$  and  $G_2$  are the tip and sample shear moduli, respectively. This convenient relationship holds for the JKR, DMT or intermediate regimes. It requires that no interfacial slip occurs, thus low lateral forces must be used for the measurement.

In an AFM experiment, the contact stiffness resides in series with the lateral cantilever stiffness. The typical lateral stiffness of commercial AFM cantilevers,  $k_{lever}$ , is around 50-200 N/m[2], which is of the same order as the lateral contact stiffness,  $k_{contact}$ , at the nanometer scale. Thus, typical cantilevers can accurately measure variations in the lateral stiffness of nanometer-sized contacts, *i.e.*

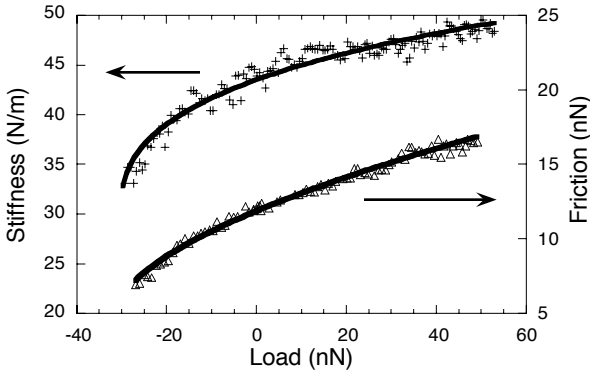


Fig. 4. Crosses: lateral stiffness ( $k_{tot}$ ) vs. load data for a  $\text{SiN}_x$  tip on mica in UHV. Triangles:  $F_f$  vs. load, acquired shortly after the stiffness measurement. Solid lines: fits of the JKR model to both measurements.

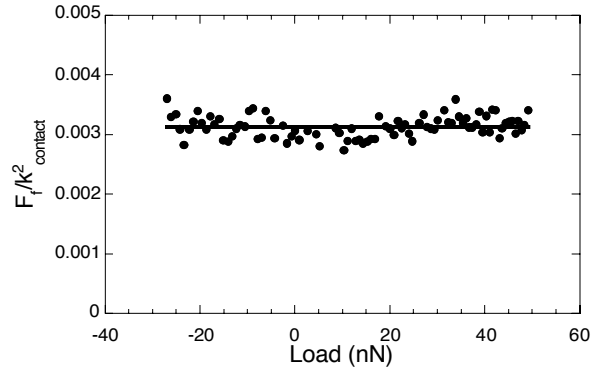


Fig. 5.  $F_f / k_{contact}^2$  vs. load for the  $\text{Si}_3\text{N}_4$  tip on mica in UHV, calculated from the stiffness and friction data in fig. 4.

$$\frac{dF_{lateral}}{dx} = k_{tot} = \left[ \frac{1}{k_{lever}} + \frac{1}{k_{contact}} \right]^{-1} \quad (6)$$

where  $F_{lateral}$  is the lateral force (cantilever torsion), and  $x$  is the lateral displacement.

The slope of the initial “sticking” portion of the tip-sample interaction during lateral sliding (fig. 2b) corresponds to  $dF_{lateral}/dx = k_{tot}$ , the total lateral stiffness. To measure this slope accurately, the relative lateral position between the cantilever base and the sample is sinusoidally modulated with an amplitude of a few Å which avoids slip even at low loads. A lock-in amplifier is used to measure the amplitude of the lateral force response over a range of loads. The in-phase response amplitude ( $dF_{lateral}$ ) divided by the amplitude of relative displacement ( $dx$ , determined by accurately knowing the piezo response calibration) corresponds to the *total* lateral stiffness of the system,  $k_{tot}$ , eq. (6). Since  $k_{lever}$  is constant,  $k_{contact}$  can be determined from this measurement.

We have measured the variation of  $k_{tot}$  with load for a  $\text{SiN}_x$  cantilever and a mica sample in UHV (fig. 4 – crosses). Indeed, a substantial variation with load is observed, due to the change in contact area. The solid line shows that the JKR model, combined with eq. (5), describes this variation quite accurately. Friction can also be measured as a function of load as described previously (fig. 4 - triangles). Again, the JKR model fits the data very well. The shear strength and adhesion energy for the interface, derived from the JKR fit, are listed in Table 1. For these calculations, we used  $E_{\text{SiN}} = 155$  GPa,  $\nu_{\text{SiN}} = 0.27$ [26]. A rather blunt paraboloidal tip of  $\sim 260$  nm radius was used for this experiment, as measured using inverse imaging.

We can verify that the shear strength is load-independent without relying on the JKR analysis. We simply divide the friction measurement at each load by the square of the corresponding contact stiffness measurement (which is proportional to the contact area). Using eqs. (4) and (5), we find

$$\frac{F_f(L)}{k_{contact}^2(L)} = \frac{\pi \cdot \tau(L)}{64 \cdot (G^*)^2} \propto \tau(L) . \quad (7)$$

This quantity is plotted vs. load in fig. 5, where we see that indeed the shear strength is load-independent over this range. Combined lateral stiffness and friction measurements can therefore determine in detail the mechanical behavior of nanometer-scale interfaces.

## WC/Diamond Interface: Contact Conductance Measurements

Diamond and tungsten-carbide are important tribological materials. Both materials generally exhibit very low friction. Diamond and diamond-like films are important coating materials used in a wide variety of tools, hard disks, micro-machines and aerospace applications. Similarly, tungsten-carbide plays an important role in several types of hard coatings. Diamond and tungsten-carbide are two of the hardest, stiffest materials known, while the adhesive forces at the interface are small due to the hydrogen passivation of the diamond surface and to the fact that carbides are generally quite inert. These properties make the system under study an excellent candidate to exhibit a DMT-like behavior for contact area *versus* load. The DMT solution for contact area is given by[22]:

$$A = \pi \left( \frac{3R}{4E^*} \right)^{2/3} \cdot (L + 2\pi R\gamma)^{2/3}. \quad (8)$$

The lateral stiffness technique described previously is not expected to work well for these materials, due to the expected low friction and high stiffness of the materials. Low friction allows slip to take place during the lateral stiffness measurement, thus underestimating the lateral stiffness response. Large elastic moduli lead to large values of  $k_{contact}$  which, as is apparent from eq. (6), cannot be sensitively measured. Since the diamond sample is boron-doped and tungsten-carbide is conductive, local contact conductance measurements can instead be performed as a function of applied load to obtain independent information about the contact area. The nanometer scale of the contact radius in AFM experiments means the total system conductance is limited by the contact and not by the bulk conductance of tip or sample. In this limit, the contact conductance becomes directly proportional to the contact area  $A$ . However, the proportionality constant is difficult to determine, preventing absolute determination of  $A$  with this technique. Nevertheless, at a fixed voltage, the current is always proportional to  $A$  for any current transport mechanism[27]. Thus, it is possible to equate the variation in current at a constant voltage to the variation in  $A$ ; this relation is used in this work.

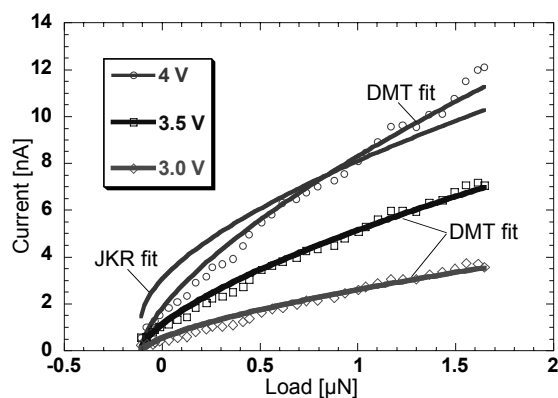


Fig. 6. The current measured through the tip-sample contact *vs.* load, at three different constant voltages. Note the accurate fit of the current to the DMT continuum mechanics model, which is proportional to the contact area.

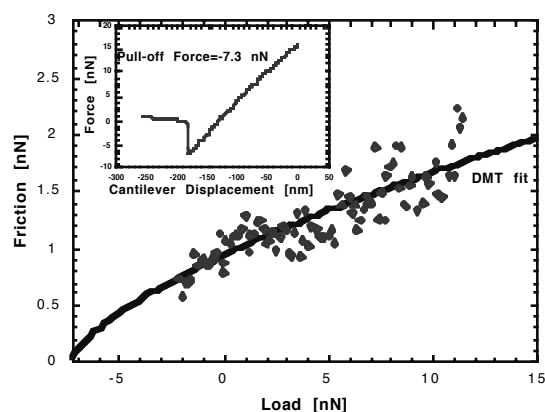


Fig. 7. Friction *vs.* load follows the same dependence as that of contact conductance *vs.* load, and therefore the same dependence as that of the DMT model, showing that friction is proportional to the contact area. The inset shows a typical force-distance curve with the pull-off force in very good agreement with the value obtained from the DMT fit.

Using a sensitive current preamplifier, the load dependence of the current at several voltages applied to the sample was measured using an 88 N/m cantilever (fig. 6). Current-voltage curves revealed consistent semiconductor-like conductance at all loads, which indicates that the conductance mechanism was not affected by the applied stress. For all bias voltages, the current vs. load data can be fit by the DMT model (solid lines). The DMT model provides an excellent fit to the measured data and the pull-off force deduced from the fits is identical to 0.1  $\mu\text{N}$  independently measured from the force-distance curves with the same lever. It is significant that the fits at all voltages have the same pull-off force, which confirms that current is proportional to contact area. These results show unambiguously that the load dependence of the contact area for this single asperity interface can indeed be described by the DMT model. As seen in fig. 6, the JKR model provides a poor fit to this data.

Friction measurements were performed using a 0.23 N/m cantilever to enhance the sensitivity to frictional forces. The radius of curvature of the paraboloidal tip was found to be  $\sim 110$  nm using inverse imaging, measured before and after tip-sample contact, thus no evidence of wear was observed. Fig. 7 shows the results of frictional force measurements as a function of applied load, which were reproducible at different locations on the sample. The data in fig. 7 were obtained by decreasing the load from 12 nN to negative loads (unloading). Experiments when the load was increased (loading) exhibited the same behavior as shown in fig. 7, indicating that the deformation of the contact is elastic for the range of loads investigated. The data in fig. 7 can be fit by the DMT model (solid line), treating both  $\gamma$  and  $\tau$  as free parameters, demonstrating that friction is proportional to  $A$ . The  $\gamma$  and  $\tau$  were determined using  $E_{\text{diamond}} = 1164$  GPa,  $\nu_{\text{diamond}} = 0.08$ [28],  $E_{\text{WC}} = 714$  GPa and  $\nu_{\text{WC}} = 0.24$ [29]. As summarized in Table 1, the DMT fit results in a pull-off force of -7.3 nN, an adhesion energy of 10 mJ/m<sup>2</sup>, and a shear strength of 238 MPa. The contact radius is 1.1 nm at zero applied load. No friction data for loads smaller than -2 nN could be obtained due to a premature pull-off of the tip at negative loads. Premature pull-off is frequently promoted by the tip-sample movement during scanning. Force-distance curves involve less lateral movement and therefore provide a direct determination of the pull-off force. The typical, reproducible result is shown in the inset of fig. 4, and the measured pull-off force of -7.3 nN is in excellent agreement with the value obtained from the DMT fit. Attempts to fit the JKR model to our friction vs. load measurements produced strongly inconsistent fits.

For the WC/diamond interface,  $G_{\text{eff}} \approx 380$  GPa, so  $\tau \approx G_{\text{eff}}/1600$ . Thus, the shear strength is relatively small in this case, especially in comparison to the Pt/mica interface. An ideal shear strength in the range of  $G/30$  requires a “crystalline” or commensurate interface. This suggests that there may be very little commensurability for the WC/diamond interface, which is plausible considering the high stiffness and weak adhesion of these materials. Further work is required to verify this hypothesis.

We do not attribute the premature pull-off described above to the partial slip phenomenon predicted by Johnson[11], as this effect is only significant for strongly adhered interfaces. van den Oetelaar has measured strong adhesion and friction between a Si tip and the clean diamond(111) surface[30], and observed that partial slip occurs with high lateral force. This was evident by a reduction of the lateral stiffness just prior to full slip.

## CONCLUSIONS

Atomic force microscopy can accurately measure load, friction, contact area, stiffness, conductance, adhesion energies, and shear strengths for nanometer-scale contacts. While careful attention must be paid to instrumental issues such as calibration, tip shape, experimental conditions and other instrumental artifacts, methods to address these issues have been developed to quite reasonable extents. Using this instrumentation, we have verified that friction at the nanometer scale, for an elastic, single asperity contact, is directly proportional to the true contact area. In other words, there appears to be a constant friction force per interfacial atom (the shear strength). The constant shear strength indicates that the mechanism of energy dissipation for these systems does not change in this range. Thus, the increase in friction with load is attributable to the increase in contact area. This may not be so surprising given that the nominal stress is only increasingly roughly as  $L^{1/3}$  (from the continuum models). New modes of energy dissipation, resulting from inelastic processes, may activate at higher stresses[1]. For example, evidence of tip-induced atomic-scale wear has been reported for alkali halide materials[31]. Pressure-activated modes of energy dissipation are reported in organic thin films due to progressive molecular deformation[32]. These examples represent stress-dependent increases in the number of energy dissipation channels and are therefore manifested in increases in the shear strength compared with purely elastic, wearless friction.

Fracture mechanics can be successfully utilized to derive continuum models that describe the contact area (as well as stress distribution, contact profile *etc.*). Impressive agreement with these continuum models is found, even at the nanometer scale. New continuum approaches to account for the effect of lateral forces on a loaded contact (using mixed-mode fracture) and the mechanism of slip (using dislocation mechanics) have been recently developed. In the AFM experiments, different relations between contact area and load are observed for different pairs of materials. The differences may also be correlated with the relative magnitude of the interfacial shear strength. Shear strengths equivalent to the ideal material strength are observed in some cases (*e.g.* Pt/mica). Nano-technology applications will require interfaces that either resist or facilitate shear, depending on the specific application. Further understanding through studies such as these could eventually allow control of these shear properties at the nanometer scale.

## ACKNOWLEDGEMENTS

We acknowledge useful discussions with K.L. Johnson, K.-S. Kim, and J. Hurtado. The Pt/mica experiments were performed and analyzed with the assistance of N. Agraït. The WC/diamond experiments were performed and analyzed with the assistance of R.J.A. van den Oetelaar and C.F.J. Flipse. R. W. C. acknowledges the support of the Natural Sciences and Engineering Research Council of Canada. This work was supported by the Director, Office of Energy Research, Basic Energy Sciences, Materials Division of the US Department of Energy under contract number DE-AC03-76SF00098.

## REFERENCES

1. R.W. Carpick and M. Salmeron, Chem. Rev. **97**, 1163 (1997).
2. D.F. Ogletree, R.W. Carpick, and M. Salmeron, Rev. Sci. Instrum. **67**, 3298 (1996).
3. Q. Dai, R. Völlmer, R.W. Carpick, D.F. Ogletree, and M. Salmeron, Rev. Sci. Instrum. **66**, 5266 (1995).
4. R.W. Carpick, N. Agraït, D.F. Ogletree, and M. Salmeron, J. Vac. Sci. Technol. B **14**, 1289 (1996).

5. S.S. Sheiko, M. Möller, E.M.C.M. Reuvekamp, and H.W. Zandbergen, *Phys. Rev. B* **48**, 5675 (1993).
6. R.W. Carpick, N. Agraït, D.F. Ogletree, and M. Salmeron, *Langmuir* **12**, 3334 (1996).
7. M. Enachescu, R.J.A. van den Oetelaar, R.W. Carpick, D.F. Ogletree, C.F.J. Flipse, and M. Salmeron, *Phys. Rev. Lett.* **81**, 1877 (1998).
8. R. van den Oetelaar and C. Flipse, *Surf. Sci.* **384**, L828 (1997).
9. S. Morita, S. Fujisawa, and Y. Sugawara, *Surf. Sci. Rep.* **23**, 3 (1996).
10. K.L. Johnson, K. Kendall, and A.D. Roberts, *Proc. Roy. Soc. London A* **324**, 301 (1971).
11. K.L. Johnson, *Proc. Roy. Soc. London A* **453**, 163 (1997).
12. D. Maugis and M. Barquins, *J. Phys. D. (Appl. Phys.)* **11**, 1989 (1978).
13. L.E. McNeil and M. Grimsditch, *J. Phys: Condens. Matter* **5**, 1681 (1992).
14. *Metals Handbook*, 10th ed. American Society for Metals, Metals Park, Ohio, 1990.
15. A.H. Cottrell, *Introduction to the Modern Theory of Metals*, Institute of Metals, London Brookfield, VT, USA, 1988.
16. J. Hurtado and K.-S. Kim, *Proc. Roy. Soc. A* **455**, 3363 (1999).
17. J. Hurtado and K.-S. Kim, Fracture and Ductile vs. Brittle Behavior - Theory, Modeling and Experiment; Proceedings of MRS Fall Meeting Symposium M, December 1998, Boston, MA. **this volume** (1999).
18. B.J. Briscoe and D.C.B. Evans, *Proc. Roy. Soc. London A* **380**, 389 (1982).
19. I.L. Singer, R.N. Bolster, J. Wegand, S. Fayeulle, and B.C. Stupp, *Appl. Phys. Lett.* **57**, 995 (1990).
20. K.L. Johnson, *Langmuir* **12**, 4510 (1996).
21. J.A. Greenwood, *Proc. Roy. Soc. London A* **453**, 1277 (1997).
22. D. Maugis, *J. Colloid Interface Sci.* **150**, 243 (1992).
23. B.V. Derjaguin, V.M. Muller, and Y.P. Toporov, *J. Colloid Interface Sci.* **53**, 314 (1975).
24. R.W. Carpick, D.F. Ogletree, and M. Salmeron, *J. Colloid Interface Sci.* **211**, 395 (1999).
25. K.L. Johnson, *Contact Mechanics*, University Press, Cambridge, 1987.
26. Dr. M. Tortonese, Park Scientific Instruments Inc., Sunnyvale, CA (personal communication).
27. S.M. Sze, *Physics of Semiconductor Devices*, 2nd ed. Wiley, New York, 1981.
28. C.A. Klein, *Materials Research Bulletin* **27**, 1407 (1992).
29. J.F. Shackelford, W. Alexander, and J.S. Park, *CRC Materials Science and Engineering Handbook*, 2nd ed. CRC Press, Boca Raton, 1994.
30. R.J.A. van den Oetelaar, Ph.D. Thesis, Eindhoven University of Technology, 1998.
31. R.W. Carpick, Q. Dai, D.F. Ogletree, and M. Salmeron, *Trib. Lett.* **5**, 91 (1998).
32. E. Barrena-Villas, S. Kopta, D.F. Ogletree, D.H. Charych, and M. Salmeron, *Phys. Rev. Lett.* **82**, 2880 (1999).